

1-1-2012

Enhanced electrochemical properties of LiFePO₄ by Mo-substitution and graphitic carbon-coating via a facile and fast microwave-assisted solid-state reaction

Dan Li

University of Wollongong, danli@uow.edu.au

Yudai Huang

Xinjiang University

Neeraj Sharma

The Bragg Institute

Zhixin Chen

University of Wollongong, zchen@uow.edu.au

Dianzeng Jia

Xinjiang University

See next page for additional authors

Follow this and additional works at: <https://ro.uow.edu.au/engpapers>

 Part of the [Engineering Commons](#)

<https://ro.uow.edu.au/engpapers/5229>

Recommended Citation

Li, Dan; Huang, Yudai; Sharma, Neeraj; Chen, Zhixin; Jia, Dianzeng; and Guo, Zaiping: Enhanced electrochemical properties of LiFePO₄ by Mo-substitution and graphitic carbon-coating via a facile and fast microwave-assisted solid-state reaction 2012, 3634-3639.
<https://ro.uow.edu.au/engpapers/5229>

Authors

Dan Li, Yudai Huang, Neeraj Sharma, Zhixin Chen, Dianzeng Jia, and Zaiping Guo

Cite this: *Phys. Chem. Chem. Phys.*, 2012, **14**, 3634–3639

www.rsc.org/pccp

PAPER

Enhanced electrochemical properties of LiFePO₄ by Mo-substitution and graphitic carbon-coating *via* a facile and fast microwave-assisted solid-state reaction†

Dan Li,^a Yudai Huang,^b Neeraj Sharma,^c Zhixin Chen,^d Dianzeng Jia^{*b} and Zaiping Guo^{*ad}

Received 20th December 2011, Accepted 18th January 2012

DOI: 10.1039/c2cp24062a

A composite cathode material for lithium ion battery applications, Mo-doped LiFePO₄/C, is obtained through a facile and fast microwave-assisted synthesis method. Rietveld analysis of LiFePO₄-based structural models using synchrotron X-ray diffraction data shows that Mo-ions substitute onto the Fe sites and displace Fe-ions to the Li sites. Supervalent Mo⁶⁺ doping can act to introduce Li ion vacancies due to the charge compensation effect and therefore facilitate lithium ion diffusion during charging/discharging. Transmission electron microscope images demonstrate that the pure and doped LiFePO₄ nanoparticles were uniformly covered by an approximately 5 nm thin layer of graphitic carbon. Amorphous carbon on the graphitic carbon-coated pure and doped LiFePO₄ particles forms a three-dimensional (3D) conductive carbon network, effectively improving the conductivity of these materials. The combined effects of Mo-doping and the 3D carbon network dramatically enhance the electrochemical performance of these LiFePO₄ cathodes. In particular, Mo-doped LiFePO₄/C delivers a reversible capacity of 162 mA h g⁻¹ at a current of 0.5 C and shows enhanced capacity retention compared to that of undoped LiFePO₄/C. Moreover, the electrode exhibits excellent rate capability, with an associated high discharge capacity and good electrochemical reversibility.

Introduction

Lithium ion batteries have been attracting widespread interest over recent decades to meet the urgent needs for applications in both fully electric vehicles and hybrid electric vehicles.^{1,2} Research into lithium iron phosphate, LiFePO₄, has been gaining momentum due to its promising electrochemical properties as a cathode material for lithium-ion batteries,^{2–5} such as its high theoretical capacity (170 mA h g⁻¹), flat voltage plateau (3.4 V vs. Li⁺/Li), and low environmental impact. These factors have allowed application of lithium-ion batteries in large-scale devices such as plug-in hybrid vehicles and electric vehicles. However, LiFePO₄ is a poor electronic

conductor, with a reported conductivity of $\sim 10^{-9}$ S cm⁻¹ at room temperature, which thus limits both diffusion and electrochemical response during lithium insertion/extraction.^{6,7} In order to improve the properties of existing LiFePO₄-based electrode materials, extensive efforts have been made by electrochemical researchers, which include particle size control and manipulation, surface modification of particles by coating with electronically conductive agents, and atomic-level doping with supervalent cations.^{8–12} Carbon coating is a common strategy to optimize the electrochemical performance of cathode materials. The carbon network restricts the growth of the LiFePO₄ particles and inhibits particle agglomeration, thereby shortening the diffusion path of lithium ions and providing a conductive bridge to the LiFePO₄ particles, which facilitates charge transfer. Wang *et al.*^{13,14} recently demonstrated, however, that a partly non-continuous carbon layer could not allow electrons to reach all the positions where Li⁺ ion intercalation took place. Therefore, the formation of a uniform and sufficient, or carefully controlled, carbon layer is essential for excellent electrochemical performance of LiFePO₄. In most cases, the coated conductive layer is amorphous^{15,16} or semi-graphitic¹³ carbon and cannot cover entire LiFePO₄ particles. A uniform graphitic carbon shell with relatively high electronic conductivity is rarely reported.

^a Institute for Superconducting and Electronic Materials, University of Wollongong, Wollongong, NSW 2522, Australia. E-mail: zguo@uow.edu.au; Tel: +61 2 4221 522 5

^b Institute of Applied Chemistry, Xinjiang University, Urumqi, Xinjiang 830046, China. E-mail: jdz0991@gmail.com

^c The Bragg Institute, Australian Nuclear Science and Technology Organisation, Locked Bag 2001, Kirrawee DC NSW 2232, Australia

^d School of Mechanical, Materials & Mechatronics Engineering, University of Wollongong, NSW 2522, Australia

† Electronic supplementary information (ESI) available: Information regarding the TGA curve for the Mo-doped LiFePO₄/C material. See DOI: 10.1039/c2cp24062a

In 2002, Chung *et al.*¹⁷ investigated different cation dopants to determine the effects of aliovalent doping on the electronic conductivity of LiFePO₄, which sparked numerous studies looking at crystallo-chemical modification of LiFePO₄. Reports indicated, *via* structural and electrochemical analyses, that cation doping could decrease the lithium miscibility gap, favor phase transformation kinetics in cycling, expand diffusion channels, and introduce controlled atomic disorder into the ordered olivine structure.¹⁰

In this work, our strategy revolves around the formation of a three-dimensional (3D) carbon network, combined with Mo⁶⁺ doping in a single synthetic procedure, in order to optimize the electrochemical performance of LiFePO₄ cathode materials. Mo-doped LiFePO₄/C nanocomposites were successfully synthesized using the facile and fast synthesis method of microwave-assisted solid-state reaction. It was found that the high valence of Mo⁶⁺ allows or promotes cation substitution onto the Fe sites, and this leads to a displacement of the corresponding quantity of Fe-ions to the Li sites, which may act to facilitate Li⁺ diffusion through one-dimensional (1D) channels along the [010] direction in combination with Li-ion vacancies. Furthermore, we speculate that Mo⁶⁺ doping leads to a change in the electronic structure of Mo-doped LiFePO₄/C due to the injection of electrons near the Fermi level,¹⁸ thus improving the electronic conductivity of the LiFePO₄/C materials. In comparison to furnace heating, the microwave-assisted solid-state method can significantly shorten the reaction time, and relatively small crystals can be obtained, reducing the diffusion path of lithium ions and further enhancing the rate performance of the material. It was also found that an *in situ* generated thin graphitic carbon layer uniformly covers individual LiFePO₄ particles, which effectively avoids undesirable particle growth and serves as an electron conductor. Furthermore, the *in situ* graphitic carbon layer connects with the surrounding amorphous carbon to form a 3D carbon network, providing an effective charge transport pathway.

Experimental

Stoichiometric quantities of CH₃COOLi·2H₂O and (NH₄)₂HPO₄ were ground in an agate mortar with a pestle for ~30 min to form a homogeneous mixture. These solid starting materials underwent a one-step solid-state reaction as reported earlier^{19–21} and morphed into a soft and pulpy mixture, and then into solid powder. FeC₂O₄·2H₂O and a small quantity of citric acid with/without Na₂MoO₄ were then added, mixed, and ground for 1 h. The molar ratio of CH₃COOLi·2H₂O to Na₂MoO₄ was 99:1. A self-assembly carbon seal reactor^{19–21} with these precursor materials inside it was then put into a microwave oven (3.0 GHz, 850 W). After 15 min of microwave irradiation, the final samples were obtained, and the powders were further milled for electrochemical testing.

The crystalline phase of the resulting materials was analyzed by powder X-ray diffraction (XRD, MXP18AHF, MAC, Japan), which was carried out using Cu K α radiation ($\lambda = 1.54056 \text{ \AA}$). Data were collected from 10 to 80° in 2θ , with a step size of 0.12° and 1.0 s per step. High-resolution synchrotron XRD (SXR) data were collected on the Powder Diffraction Beamline (10-BM-1)²² at the Australian Synchrotron using a wavelength (λ) of 0.68788(2) Å, determined using the National

Institute of Standards and Technology (NIST) 660a LaB₆ standard reference material. Powder samples were packed and sealed in 0.5 mm glass capillaries, and data were collected for 6 minutes at ambient temperature using Debye–Scherrer geometry. Thermogravimetric analysis (TGA) was carried out to determine the carbon content with a TGA/DSC type instrument (METTLER TOLEDO, Switzerland) at a heating rate of 10 °C min⁻¹ from room temperature to 800 °C in air. Transmission electron microscope (TEM) investigations were performed using a JEOL 2011F analytical electron microscope (JEOL, Tokyo, Japan) operating at 200 keV. X-Ray photoelectron spectroscopy (XPS) experiments were carried out on a VG Scientific ESCALAB 220IXL instrument using aluminium K α X-ray radiation during XPS analysis.

To prepare the working electrode for electrochemical testing, a cathode slurry was prepared by thoroughly mixing 85 wt% active material, 10 wt% acetylene black, and 5 wt% poly(vinylidene fluoride) (PVdF) in *N*-methyl pyrrolidinone (NMP) solvent. The cathode slurry was then spread onto aluminium foil substrates and dried in a vacuum oven at 120 °C for 12 h. The electrochemical tests were carried out on CR2032 coin type cells. The cells were constructed of a lithium foil anode, the prepared active material on aluminium as a cathode, microporous polyethylene (Celgard 2400) as the separator, and 1 M LiPF₆ in a mixture of ethylene carbonate (EC) and dimethyl carbonate (DMC) (1:1 by volume) as the electrolyte. The whole assembly process was carried out in an argon-filled glove box. Cyclic voltammograms (CVs) were collected from 2.5 to 4.1 V using a CHI660B electrochemical workstation (CHI, 660B, CHENHUA, China). The charge/discharge cycling was performed within a voltage range of 2.5–4.1 V on a battery test instrument (CT2001A, KINGNUO, China) at ambient temperature.

Results and discussion

XRD patterns of the as-prepared LiFePO₄/C and Mo-doped LiFePO₄/C are shown in Fig. 1. The presence of sharp and well-defined Bragg peaks, which visually match the expected reflections from the olivine LiFePO₄ structure, suggests the presence of crystalline products.²³ No significant signal was associated with carbon, which indicates that the residual carbon is amorphous or that the carbon layer on LiFePO₄ particles is thin.²⁴ The carbon content in the obtained Mo-doped

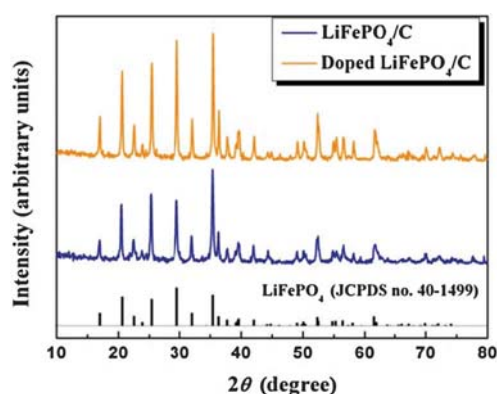


Fig. 1 XRD patterns of LiFePO₄/C before and after Mo doping. The vertical lines mark the reflections in the standard.

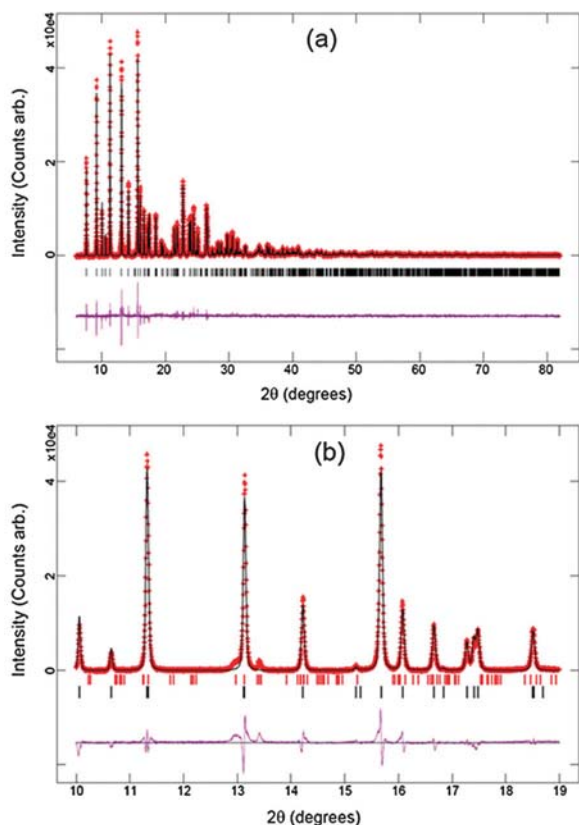


Fig. 2 (a) Rietveld-refined fit of the LiFePO_4 -based model from synchrotron X-ray diffraction data, with $R_p = 4.32\%$, $wR_p = 5.81\%$, $R_F^2 = 10.42\%$, and $\chi^2 = 2.67$. (b) Enlarged region highlighting the quality of the fit and the presence of the second phase, $\text{Li}_3\text{Fe}_2(\text{PO}_4)_3$. Observed data (for Mo-doped LiFePO_4/C) are shown as crosses (+), the calculated model as a solid line, and the difference as a solid line below. Vertical black lines indicate Bragg reflections corresponding to LiFePO_4 , and vertical red lines in (b) indicate Bragg reflections corresponding to $\text{Li}_3\text{Fe}_2(\text{PO}_4)_3$.

or undoped LiFePO_4/C is about 12 wt% by thermogravimetric analysis (see Fig. S1, ESI[†]). High resolution SXRDX data were collected on the doped sample, and the Rietveld-refined model of LiFePO_4 fitted to the SXRDX data is shown in Fig. 2(a). Fig. 2(b) clearly demonstrates that there is a small but identifiable impurity

of $\text{Li}_3\text{Fe}_2(\text{PO}_4)_3$ in the synthesized sample. To model molybdenum substitution into the LiFePO_4 , we first incorporate Mo on the Li site in the ideal LiFePO_4 model and observe a corresponding decrease in the Rietveld refinement statistics of the Bragg R -factor of $R_F^2 = 0.05\%$, while the remaining statistics, the profile factor (R_p), weighted profile factor (wR_p), and goodness-of-fit term (χ^2), remain virtually constant. Substituting Mo on the Fe site, *i.e.* $\text{Li}_{0.99}\text{Fe}_{0.01}[\text{Fe}_{0.99}\text{Mo}_{0.01}]\text{PO}_4$, however, results in a decrease in all the refinement statistics ($R_F^2 = 0.20\%$, $R_p = 0.02\%$, $wR_p = 0.03\%$, and $\chi^2 = 0.02$) with the use of the same number of parameters. The Li/Mo mixed site atomic displacement parameters (ADPs) also gave reasonable values relative to the larger values found in the earlier models. Although accuracy in the lithium occupation is difficult to determine with XRD techniques, the refinement of the lithium occupation with this dataset results in a composition of $\text{Li}_{0.96(2)}\text{Fe}_{0.01}[\text{Fe}_{0.99}\text{Mo}_{0.01}]\text{PO}_4$, which suggests a high valence of molybdenum in the sample, using these charge balance considerations. Mo-ions substitute onto the Fe site in the LiFePO_4 crystal structure, with the corresponding content of Fe being displaced onto the Li site. We propose that there is Li-ion vacancy charge compensation on the Li site, which can further facilitate enhanced Li-ion diffusion. Note that Fe or Mo ions on the Li site can be intuitively considered to be detrimental to electrochemical properties because the [010] channel could be blocked by less mobile ions (Mo^{6+} in our case). Chiang *et al.* present an argument, which is further based on subsequent theoretical calculations, considering the particle size and doping level, that demonstrates that the [010] channel could remain open for Li extraction and insertion if the particle size is small enough (less than a few tens of nanometres) and the doping level is low (a few percent).¹⁰ Considering the small crystal size (30–50 nm as shown in the high resolution TEM (HRTEM) image in Fig. 3(b)) and the low doping level (1%) in the Mo-doped LiFePO_4/C , we propose that the channel blocking effect of the Mo ions is likely to be negligible and that such an effect would easily be overcome by the presence of Li-ion vacancies.

The particle size and morphology of the Mo-doped LiFePO_4/C were characterized by TEM, as shown in Fig. 3. An HRTEM image is shown in Fig. 3(b), which clearly reveals that the particle size of Mo-doped LiFePO_4/C is in the range of 30–50 nm, and that the particles are completely covered by a thin layer of carbon (5 nm) to form a LiFePO_4/C core-shell structure. The fast and

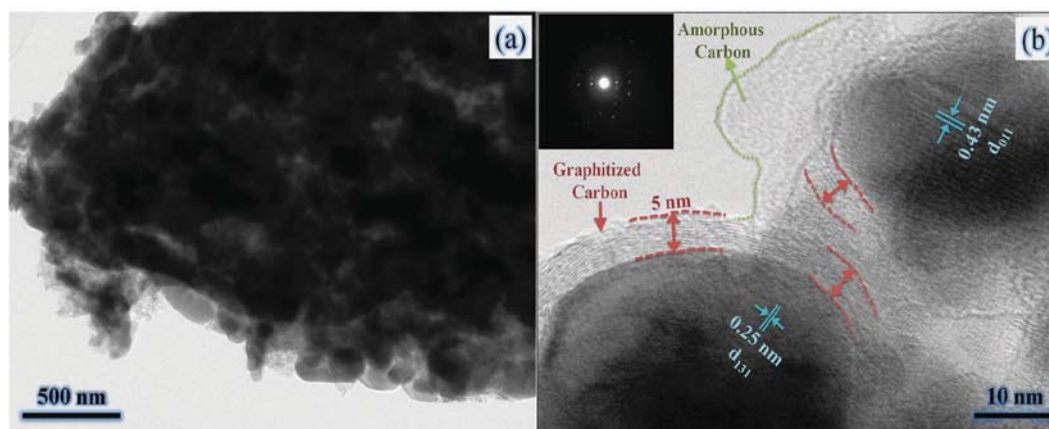


Fig. 3 TEM images of the Mo-doped LiFePO_4/C sample: (a) typical TEM image, (b) HRTEM image and corresponding SAED pattern (inset).

effective microwave heating leads to small LiFePO_4 particles and *in situ* coating of carbon on the particles, which readily inhibits agglomeration and further crystal growth. It is interesting to note that the carbon shell, which is thin enough to allow penetration of lithium ions, is graphitic carbon within a larger amorphous carbon network. Therefore, this can be considered as a specialized double carbon structure, *i.e.* graphitic carbon shells uniformly covering the surfaces of the individual LiFePO_4 particles and an amorphous carbon surrounding region.

The latter plays the role of bridging the LiFePO_4 particles to form a 3D electronically conductive interconnected network, which will significantly enhance the electronic conductivity of the material. The 3D carbon network could also ensure that electron transport occurs in all directions towards the locations of lithium ion insertion/extraction. In Fig. 3(b), the 0.25 nm and 0.43 nm lattice fringes were indexed to the (131) and (011) planes, respectively, of orthorhombic LiFePO_4 . The inset of Fig. 3(b) shows the corresponding selected area electron diffraction (SAED) pattern, indicating the highly crystalline nature of the sample.

X-Ray photoelectron spectra exhibiting Mo, C, and all the elements of LiFePO_4 are shown in Fig. 4. Li 1s could not be seen clearly because it is superimposed on the Fe 3p peak at about 56 eV.²⁵ The binding energy of P 2p, C 1s, and O 1s was determined to be 133.7 eV, 284.9 eV, and 531.6 eV, respectively. A satellite peak to the main Fe $2p_{3/2}$ peak (711.6 eV) at the higher binding energy of 716.3 eV was observed in the Mo-doped LiFePO_4/C samples. The appearance of this satellite peak is a characteristic feature of transition metal ions with partially filled d-orbitals.²⁶ The high-resolution XPS spectrum of Mo 3d shows peaks centered at 232.6 eV and 235.7 eV, corresponding to $\text{Mo}^{6+} 3d_{5/2}$ and $\text{Mo}^{6+} 3d_{3/2}$, respectively, further verifying the presence of Mo^{6+} in the obtained sample.²⁷ A non-stoichiometric cation ratio and Li-ion vacancies in LiFePO_4 may be induced in order

to accommodate the introduction of the supervalent Mo^{6+} . This, in turn, can facilitate lithium ion diffusion in these channels and therefore enhance the electrochemical performance.

Electrochemical measurements confirm the hypothesis that Mo-doping improves performance as proposed above. Fig. 5(a) shows a comparison of the rate performance of the LiFePO_4/C and the Mo-doped LiFePO_4/C samples in the potential range of 2.5–4.1 V. The capacities of both samples decrease with increasing current rate, which is associated with the supply of electrons to the active components in the cathode. The discharge capacity of LiFePO_4/C is 134 mA h g^{-1} in the first cycle at 0.5 C (where the current density of the 1 C rate is 170 mA g^{-1}) and decreases to 126 mA h g^{-1} after 20 cycles at 1 C. Specific capacities of 118, 112, 107, and 97 mA h g^{-1} were obtained at current rates of 2.5 C, 4 C, 5 C, and 7.5 C, respectively. For the Mo-doped sample, however, the boundaries to the measured capacities at different current rates (0.5 C, 1 C, and 2.5 C) are not very distinct. After 180 cycles, the discharge capacity drops from 139 mA h g^{-1} (2.5 C) to 128 mA h g^{-1} (5 C). Even at a rate of 7.5 C, a reversible capacity of 116 mA h g^{-1} for Mo-doped LiFePO_4/C can still be achieved, whereas the value for LiFePO_4/C is 97 mA h g^{-1} . In addition, the original capacity for both samples can be recovered with application of the original current rate of 0.5 C, revealing that the two synthesized samples possess good electrochemical reversibility. The good capacity and high rate capability indicate high electronic conductivity and lithium ion diffusion in the LiFePO_4/C samples, especially the Mo-doped sample, throughout lithiation/delithiation.¹⁷ Fig. 5(b) shows representative charge/discharge profiles of the Mo-doped LiFePO_4/C as a function of the specific capacity for current rates ranging from 0.5 C to 7.5 C. The discharge capacity decreases as the current rate increases, and simultaneously, the polarization in the charge/discharge curves becomes more pronounced. The Mo-doped LiFePO_4/C electrode

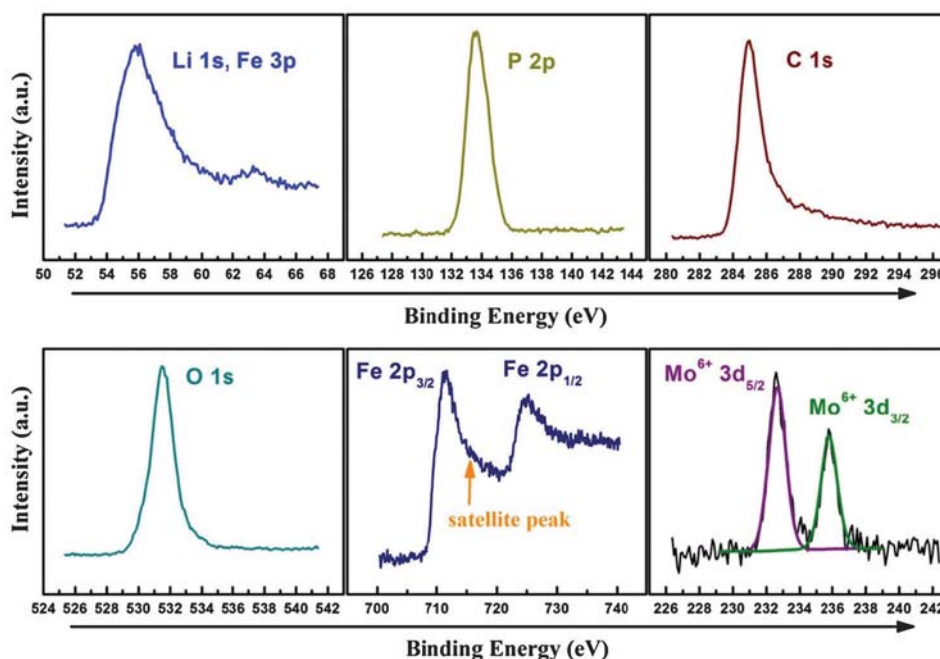


Fig. 4 XPS spectra of all elements of the Mo-doped LiFePO_4/C sample.

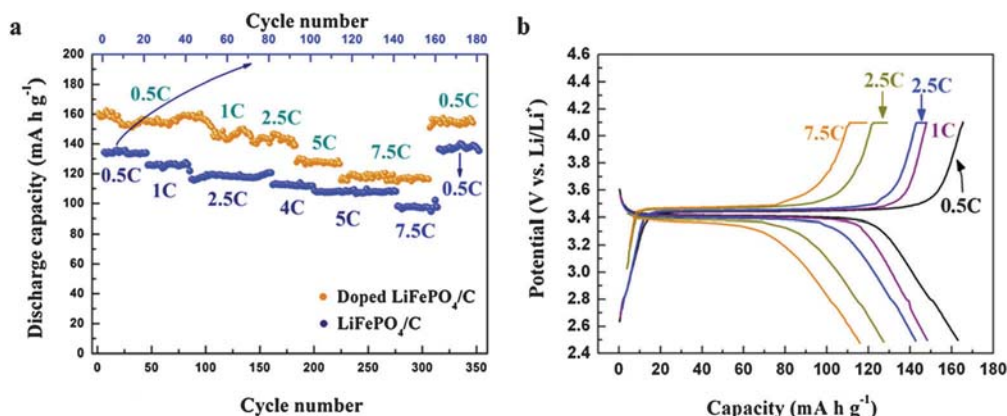


Fig. 5 (a) Reversible capacities during continuous cycling at various discharge rates of LiFePO₄/C and Mo-doped LiFePO₄/C electrodes, (b) typical charge/discharge profiles of Mo-doped LiFePO₄/C at different discharge rates.

delivers a specific capacity of 162 mA h g⁻¹ at 0.5 C with a voltage plateau at about 3.4 V vs. Li/Li⁺, and there is only a slight discrepancy in potential between the charge and discharge curves. The capacities obtained were 149 mA h g⁻¹ at 1 C, 142 mA h g⁻¹ at 2.5 C, 124 mA h g⁻¹ at 5 C, and 118 mA h g⁻¹ at 7.5 C. The electrochemical performance of Mo-doped LiFePO₄/C is better than that of the LiFePO₄/C nanocomposite with a core-shell structure reported by Wang *et al.*,¹³ the carbon-coated single crystalline LiFePO₄ by Zhu *et al.*,²⁸ and the LiFePO₄/C composite by Zhang *et al.*²⁷ which also applied Mo substitution in LiFePO₄. Comparable electrochemical performance has been obtained for the double-carbon-coated LiFePO₄ reported by Oh *et al.*²⁹ This report, however, used a complicated technique of double carbon coating that significantly limits the application of electroactive materials. The excellent electrochemical performance of Mo-doped LiFePO₄/C at a high current rate can be attributed to: (1) the graphitic carbon coating and the 3D carbon conductive network, which are postulated to significantly improve the electronic conductivity of the material; (2) Mo-doping, which induces or results in Li-ion vacancies, facilitating enhanced lithium ion diffusion; and (3) the relatively small particles fabricated by the fast and effective microwave-assisted solid-state reaction, which reduces the lithium ion diffusion path lengths. The as-prepared Mo-doped LiFePO₄/C also exhibits excellent cycling performance, with no obvious discharge capacity loss over 2500 cycles at both current rates of 1 C and 5 C, as shown in Fig. 6. In the first 50 cycles, the cell was charged and discharged at a rate of 1 C, and the capacity increased slightly with cycling. There is obvious fluctuation in capacity, which may be caused by the temperature change during testing and the equipment used. In order to show the amplitude of the fluctuation, Fig. 6(c) and (d) shows the enlarged cycling data for 250–400 and 2250–2500 cycles, respectively. Fig. 6(e) presents the charge/discharge curves of the Mo-doped LiFePO₄/C for various cycles. A flat 3.4 V voltage plateau vs. Li/Li⁺ is still observed, even at the 2500th cycle, demonstrating the excellent electrochemical performance of the electrode. The difference between charge potential and discharge potential (ΔE) is only minor, which suggests low polarization of the electrode. This is confirmed by the cyclic voltammograms in Fig. 7.

In order to further illustrate the effects of Mo doping on the electrochemical properties, Fig. 7 compares cyclic voltammograms

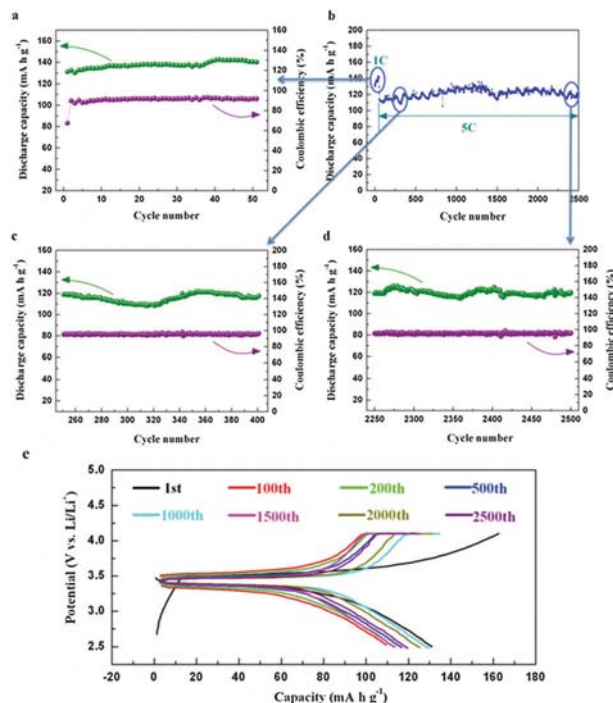


Fig. 6 (b) Cycling profiles of Mo-doped LiFePO₄/C tested at 1 C in the first 50 cycles and 5 C in the following cycles between 2.5 and 4.1 V; (a), (c), and (d) show the capacity and coulombic efficiency as a function of cycle number, covering the 1st to the 50th cycle, the 250th to the 400th cycle, and the 2250th to the 2500th cycle, respectively. (e) Charge/discharge curves for selected cycles.

of LiFePO₄/C and Mo-doped LiFePO₄/C at the scan rate of 0.1 mV s⁻¹. Both curves exhibit equilibrium anodic potentials at about 3.5 V and cathodic potentials at around 3.4 V vs. Li⁺/Li, corresponding to the extraction and insertion of lithium ions from LiFePO₄, respectively. The voltage separation between cathodic and anodic peaks is usually considered to show the reversibility of the electrochemical reaction. Clearly a narrower peak separation and higher peak current are observed for Mo-doped LiFePO₄/C relative to the undoped LiFePO₄/C, indicating better reversibility and reduced polarization *via* Mo doping.

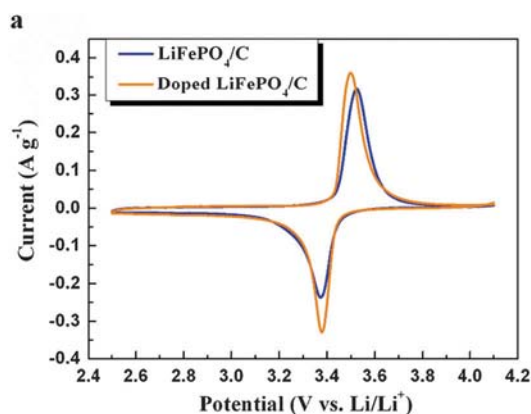


Fig. 7 Cyclic voltammograms of LiFePO₄/C and Mo-doped LiFePO₄/C at the scan rate of 0.1 mV s⁻¹.

Conclusions

Mo-doped LiFePO₄/C composite cathode material has been synthesized *via* a facile and fast microwave-assisted solid-state reaction. Rietveld analysis shows the incorporation of Mo onto the Fe site in the LiFePO₄ crystal structure, with the corresponding content of Fe being displaced onto the Li site. The Li-ion vacancies that are consequently formed also act to facilitate lithium ion diffusion, which can enhance the electrochemical performance of LiFePO₄. The relatively small particle size, generated by the fast and effective microwave assisted synthesis, reduces the diffusion path of the lithium ions. The uniform graphitic carbon coating on the Mo-doped LiFePO₄/C and the 3D carbon network improve electronic conductivity. The combination of these three effects effectively enhances the electrochemical performance of Mo-doped LiFePO₄/C. The Mo-doped LiFePO₄/C electrode, when charged and discharged at a constant current rate of 0.5 C, exhibits a capacity of 162 mA h g⁻¹. The sample further demonstrates a steady capacity of about 120 mA h g⁻¹ over 2500 cycles at the 5 C current rate, suggesting excellent cycling performance. The Mo-doped LiFePO₄/C reported here shows good properties for application as a cathode material in high-power lithium batteries.

Acknowledgements

This work was funded by the Australian Research Council (ARC) through a Discovery project (DP1094261). The authors also would like to thank Dr Tania Silver at the University of Wollongong for critical reading of the manuscript.

Notes and references

- 1 A. K. Padhi, K. S. Nanjundaswamy and J. B. Goodenough, *J. Electrochem. Soc.*, 1997, **144**, 1188–1194.
- 2 P. P. Prosini, D. Zane and M. Pasquali, *Electrochim. Acta*, 2001, **46**, 3517–3523.
- 3 K.-F. Hsu, S.-Y. Tsay and B.-J. Hwang, *J. Power Sources*, 2005, **146**, 529–533.
- 4 A. K. Padhi, K. S. Nanjundaswamy and J. B. Goodenough, *J. Electrochem. Soc.*, 1997, **144**, 1188–1194.
- 5 A. Yamada, S. C. Chung and K. Hinokuma, *J. Electrochem. Soc.*, 2001, **148**, A224–A229.
- 6 Y. Wang and G. Cao, *Adv. Mater.*, 2008, **20**, 2251–2269.
- 7 K.-S. Park, S. B. Schougaard and J. B. Goodenough, *Adv. Mater.*, 2007, **19**, 848–851.
- 8 P. S. Herle, B. Ellis, N. Coombs and L. F. Nazar, *Nat. Mater.*, 2004, **3**, 147–152.
- 9 M. S. Song, Y. M. Kang, J. H. Kim, H. S. Kim, D. Y. Kim, H. S. Kwon and J. Y. Lee, *J. Power Sources*, 2007, **166**, 260–265.
- 10 N. Meethong, Y.-H. Kao, S. A. Speakman and Y.-M. Chiang, *Adv. Funct. Mater.*, 2009, **19**, 1060–1070.
- 11 H. Liu, Q. Cao, L. J. Fu, C. Li, Y. P. Wu and H. Q. Wu, *Electrochem. Commun.*, 2006, **8**, 1553–1557.
- 12 C. A. J. Fisher and M. S. Islam, *J. Mater. Chem.*, 2008, **18**, 1209–1215.
- 13 Y. Wang, Y. Wang, E. Hosono, K. Wang and H. Zhou, *Angew. Chem., Int. Ed.*, 2008, **47**, 7461–7465.
- 14 Y.-S. Hu, Y.-G. Guo, R. Dominko, M. Gaberscek, J. Jamnik and J. Maier, *Adv. Mater.*, 2007, **19**, 1963–1966.
- 15 C. Sun, S. Rajasekhara, J. B. Goodenough and F. Zhou, *J. Am. Chem. Soc.*, 2011, **133**, 2132–2135.
- 16 J. Zhao, J. He, J. Zhou, Y. Guo, T. Wang, S. Wu, X. Ding, R. Huang and H. Xue, *J. Phys. Chem. C*, 2011, **115**, 2888–2894.
- 17 S.-Y. Chung, J. T. Bloking and Y.-M. Chiang, *Nat. Mater.*, 2002, **1**, 123–128.
- 18 Z. Wang, S. Sun, D. Xia, W. Chu, S. Zhang and Z. Wu, *J. Phys. Chem. C*, 2008, **112**, 17450–17455.
- 19 L. Wang, Y. Huang, R. Jiang and D. Jia, *J. Electrochem. Soc.*, 2007, **154**, A1015–A1019.
- 20 L. Wang, Y. Huang, R. Jiang and D. Jia, *Electrochim. Acta*, 2007, **52**, 6778–6783.
- 21 D. Li, Y. Huang, D. Jia, Z. Guo and S.-J. Bao, *J. Solid State Electrochem.*, 2009, **14**, 889–895.
- 22 K. S. Wallwork, B. J. Kennedy and D. Wang, *AIP Conf. Proc.*, 2007, **879**, 879–882.
- 23 N. Jayaprakash and N. Kalaiselvi, *Electrochem. Commun.*, 2007, **9**, 620–628.
- 24 L.-L. Zhang, G. Liang, A. Ignatov, M. C. Croft, X.-Q. Xiong, I. M. Hung, Y.-H. Huang, X.-L. Hu, W.-X. Zhang and Y.-L. Peng, *J. Phys. Chem. C*, 2011, **115**, 13520–13527.
- 25 J. Xu, G. Chen, C. Xie, X. Li and Y. Zhou, *Solid State Commun.*, 2008, **147**, 443–446.
- 26 M. S. Bhuvaneshwari, N. N. Bramnik, D. Enslin, H. Ehrenberg and W. Jaegermann, *J. Power Sources*, 2008, **180**, 553–560.
- 27 M. Zhang, L.-F. Jiao, H.-T. Yuan, Y.-M. Wang, J. Guo, M. Zhao, W. Wang and X.-D. Zhou, *Solid State Ionics*, 2006, **177**, 3309–3314.
- 28 C. Zhu, Y. Yu, L. Gu, K. Weichert and J. Maier, *Angew. Chem., Int. Ed.*, 2011, **50**, 6278–6282.
- 29 S. W. Oh, S.-T. Myung, S.-M. Oh, K. H. Oh, K. Amine, B. Scrosati and Y.-K. Sun, *Adv. Mater.*, 2010, **22**, 4842–4845.